Available online at www.sciencedirect.com
SCIENCE DIRECT
International Journal of Heat and Mass Transfer 49 (2006) 1039–1049
International Journal of HEAT and MASS TRANSFER
www.elsevier.com/locate/ijhmt

Numerical simulation of natural convection heat transfer in a porous cavity heated from below using a non-Darcian and thermal non-equilibrium model

S.A. Khashan [a], A.M. Al-Amiri [a], I. Pop [b,*]

[a] Mechanical Engineering Department, United Arab Emirates University, P.O. Box 17555, Al-Ain, United Arab Emirates
[b] University of Cluj, Faculty of Mathematics, R-3400 Cluj, CP 253, Romania

Received 14 September 2005
Available online 5 December 2005

Abstract

The present paper investigates the numerical simulation of steady laminar incompressible natural convection heat transfer in an enclosed cavity that is filled with a fluid-saturated porous medium. The bottom wall is subjected to a relatively higher temperature than the top wall while the vertical walls are considered to be insulated. The flow field is modeled upon incorporating different non-Darcian effects, such as the convective term, Brinkman effect and Forchhiemer quadratic inertial effect. Moreover the two-equation model is used to separately account for the local fluid and solid temperatures. The numerical solution is obtained through the application of the finite volume method. The appraisals of the sought objectives are performed upon identifying key dimensionless groups of parameters. These dimensionless groups along with their operating domains are: Rayleigh number $1 \leqslant Ra \leqslant 400$, Darcy number $10^{-4} \leqslant Da \leqslant 10^{-3}$, effective fluid-to-solid thermal conductivity ratio $0.1 \leqslant \kappa \leqslant 1.0$, and the modified Biot number $1 \leqslant \chi \leqslant 100$. The non-Darcian effects are first examined over a broad range of Rayleigh number. Next, the implications of the group of parameters on the flow circulation intensity, local thermal non-equilibrium (LTNE) and average Nusselt number are highlighted and pertinent observations are documented.

Keywords: Porous medium; Natural convection; Non-Darcy model; Local thermal non-equilibrium model; Numerical simulation

1. Introduction

Natural convection in a fluid-saturated porous medium is of significant interest to researchers owing to its various applications in different fields such as geothermal energy modeling, thermal insulation material, cooling of electronic devices and solar receivers to name a few. Several excellent monographs summarizing the state-of-the-art available in the literature testify to the maturity of this area, see for example, Nield and Bejan [1], Ingham and Pop [2], Vafai [3], Pop and Ingham [4], Bejan and Kraus [5], Ingham et al. [6] and Bejan et al. [7].

The buoyancy-driven convection associated with a cavity heated from below brings about patterns of convection cells. In each cell, the fluid rotates in a closed orbit and the direction of rotation alternates with successive cells. This phenomenon is conventionally referred to in the literature as the Bénard convection. Such a convection phenomenon also receives a broad attention owing to the inherited hydrodynamic fluid stability. The critical Rayleigh number, which signals the onset of natural convection, was first reported by Lapwood [8] to be equal to $4\pi^2$ for a Darcy fluid flow in a porous medium bounded between two infinite horizontal surfaces maintained at two different isothermal temperatures.

The presence of a porous medium inside the cavity hinders the buoyancy-driven activities. In essence, the momentum transport process in a porous medium is governed by several inherited phenomena such as the non-Darcian

* Corresponding author. Tel.: +40 264 594315; fax: +40 264 591906.
E-mail address: popi@math.ubbcluj.ro (I. Pop).

0017-9310/$ - see front matter © 2005 Elsevier Ltd. All rights reserved.
doi:10.1016/j.ijheatmasstransfer.2005.09.011

Nomenclature

A	aspect ratio, L/H
a_{sf}	specific surface area (m^2/m^3)
c_f	fluid specific heat (J/(kg K))
Da	Darcy number, K/H^2
F	inertia coefficient
h_{sf}	interstitial heat transfer coefficient ($W\ m^{-2}\ K^{-1}$)
H	cavity height (m)
k	thermal conductivity ($W\ m^{-1}\ K^{-1}$)
k_m	modified thermal conductivity, $\varepsilon k_f + (1-\varepsilon)k_s$
K	permeability (m^2)
L	cavity length (m)
P	dimensionless pressure, $pH^2/\rho_f\alpha_m^2$
p	pressure (kPa)
Pr	Prandtl number, ν_f/α_f
Ra	Rayleigh–Darcy number, $g\beta(T_h - T_c)H^3Da/\nu_f\alpha_m$
T	intrinsic average fluid or solid temperature (K)
u, v	interstitial velocity components (m/s)
$\mathbf{v}$	interstitial velocity vector (m/s)
$\mathbf{V}$	dimensionless interstitial velocity vector, $\mathbf{v}H/\alpha_m$
U, V	dimensionless interstitial velocity components
x, y	spatial axial and transverse coordinates (m)
X	dimensionless axial coordinates, x/H
Y	dimensionless radial coordinates, y/H
α_f	thermal diffusivity $(k/\rho c)_f$
α_m	modified thermal diffusivity, $k_m/(\rho c)$
χ	modified Biot number, $h_{sf}a_{sf}H^2/k_m$
ε	porosity (m^3/m^3)
κ	effective fluid-to-solid thermal conductivity ratio, k_{feff}/k_{seff}
ν_f	fluid kinematic viscosity ($m^2\ s^{-1}$)
ρ_f	fluid density (kg/m^3)
θ	dimensionless temperature, $(T - T_c)/(T_h - T_c)$
Ψ	dimensionless stream function

Subscripts

c	cold
eff	effective
f	fluid
h	hot
s	solid

effects. These non-Darcian effects represent deviations from the familiar Darcy's law. Such non-Darcian effects include the viscous and quadratic inertial effects and the spatial-porosity variation effect. In addition, the modeling of the energy transport mechanism in a porous medium has its own share of challenging fronts. For example, the flow through the tortuous paths of a porous structure offers flow recirculation and mixing, which is classified in the literature under thermal dispersion effect. Moreover, modeling of a porous medium transport coefficient, i.e., energy carrier involves various presumptions and theories. Such challenges serve as ingredients for a wide debate and discussion over the appropriate modeling of the various effects, which is reflected in the large number of publications cited in the literature in this regard. The work of Kaviany [9], Nield and Bejan [1] and Vafai [3] can be cited as lead references in this regard.

The implications of the quadratic inertia term and the viscous term on natural convection heat transfer were tackled, for instance, by Chan et al. [10] and Lauriat and Prasad [11]. Also, the impact of Prandtl number on the Bénard convection was numerically investigated by Georgiadis and Catton [12] and Lage et al. [13]. Vasseur et al. [14] conducted a numerical simulation using the Darcy–Brinkman model to study the flow and thermal behaviors in a shallow cavity subjected to a uniform heating and cooling through opposite walls. Their results demonstrated the dependence of the Nusselt number predictions on the Darcy–Rayleigh number and Darcy number. Furthermore, Beji and Gobin [15] and Al-Amiri [16] have discussed the contribution of thermal dispersion to the overall natural convection heat transfer mechanism. Such an effect is customarily modeled as a diffusive term added to the effective thermal conductivity of the fluid phase. Both studies reported an appreciated increase in the computed Nusselt number upon incorporating thermal dispersion effect and better agreement with experimental results as well.

It is customary to handle the modeling of transport phenomena inside porous media using the volume-averaging method. The work of Vafai and Tien [17] is widely recognized for using the volume-averaging technique coupled with semi-empirical formulas to arrive at the two-dimensional momentum equation, which would complement the empirical energy conservation equation. The work of Khashan et al. [18] has elaborated on the implementation of the above method.

Our review of literature has indicated that most of the reported studies on Bénard convection had resorted to local thermal equilibrium (LTE) model, which presumes that the fluid and the solid phases are defined by a unique temperature at a given location within the porous medium. Such an assumption cannot be justified, however, when the temperature difference between the two phases is considered a crucial design parameter such as, for example, in porous metal heat exchangers and nuclear fluid rods placed in a coolant bath (see [19]). When the local fluid and solid phase temperatures are accounted for separately, two energy equations emerge to represent each phase. These equations supplemented with an additional term that models the modes of heat transfer between the two phases. In a series of studies spear-headed by Amiri and co-workers [20–22], the validity of local thermal equilibrium assump-

tion and its domain of applicability was thoroughly discussed and explored under various selected scenarios.

The motivation behind the present work is to examine the severity of the local thermal equilibrium assumption in a shallow cavity filled with a fluid-saturated porous medium subjected to isothermal heating and cooling from below and above, respectively. Four different flow field models are considered in this regard, namely; the Darcy model, Darcy–Brinkman model, Darcy–Brinkman with convective term and the generalized form of the momentum equation, which accounts for the flow convective, viscous and inertial effects. In addition, the governing equations are discretized using the finite volume method while employing the primitive variables approach. Furthermore, the significance of the local thermal non-equilibrium (LTNE) model along with flow circulation intensity and Nusselt number predictions are examined over a broad range of dimensionless groups such as the Rayleigh number, Darcy number, effective fluid-to-solid thermal conductivity ratio and the modified Biot number, i.e., dimensionless interstitial heat transfer.

2. Mathematical formulation

The current investigation addressed the momentum and energy transport phenomena of a steady natural convective flow inside a two-dimensional cavity filled with a fluid-saturated porous medium. The fluid is a Newtonian incompressible fluid ($Pr = 0.7$) that operates under the laminar regime. The cavity walls are assumed to be rigid, impermeable and non-conducting. Furthermore, the porous medium is considered to be homogenous and isotropic throughout the cavity with a porosity value of $\varepsilon = 0.9$. The schematic configuration of the problem is illustrated in Fig. 1, where H and L denote the height and length of the cavity, respectively. A shallow cavity with an aspect ratio $A = L/H = 5$ is considered in the current investigation. Moreover, it is assumed that the onset of natural convection takes place keeping the horizontal bottom wall to a relatively higher temperature T_h than its top counterpart T_c, whereas the vertical walls are assumed to be insulated. The physical properties of the working fluid and the solid matrix are taken to be constant except for the density variation in the buoyancy force, which is treated according to the Boussinesq approximation.

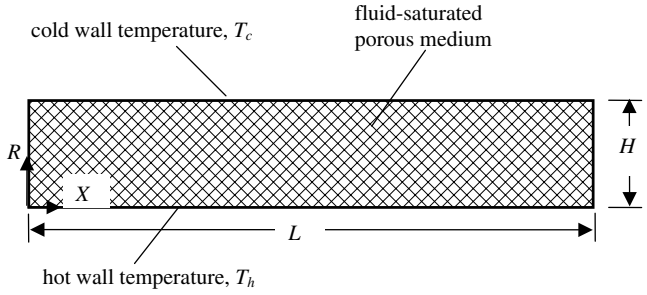

Fig. 1. Schematic representation of the porous cavity.

The variation in the local fluid and solid phase temperatures are considered throughout the porous cavity except at the solid boundaries. Accordingly, each phase is represented by a separate energy equation. In addition, the energy communication between the two phases is assumed solely attributed to a convective mode of heat transfer. Viscous dissipation, heat generation and pressure work are all assumed to have negligible effect on the velocity and temperature fields and, thus, are neglected.

The steady state modeling of the governing equations for mass, momentum and energy is based on volume-averaging method and is presented here in canonical forms as outlined by Amiri and Vafai [20]

$$\nabla \cdot \langle \mathbf{v} \rangle = 0 \tag{1}$$

$$\frac{1}{\varepsilon^2}\langle (\mathbf{v}\cdot\nabla)\mathbf{v}\rangle = -\frac{1}{\rho_f}\nabla\langle p\rangle^f + \frac{\nu_f}{\varepsilon}\nabla^2\langle \mathbf{v}\rangle - \frac{\nu_f\langle \mathbf{v}\rangle}{K} - \frac{F}{K^{1/2}}|\langle \mathbf{v}\rangle|\langle \mathbf{v}\rangle - \beta(\langle T_f\rangle^f - T_c)\mathbf{g} \tag{2}$$

$$\varepsilon(\rho c)_f \mathbf{v}\cdot\nabla\langle T_f\rangle^f = \nabla\cdot(k_{feff}\cdot\nabla\langle T_f\rangle^f) + h_{sf}a_{sf}(\langle T_s\rangle^s - \langle T_f\rangle^f) \tag{3}$$

$$\nabla\cdot(k_{seff}\cdot\nabla\langle T_s\rangle^s) - h_{sf}a_{sf}(\langle T_s\rangle^s - \langle T_f\rangle^f) = 0 \tag{4}$$

where a_{sf} is the interstitial surface area per unit volume of a porous medium, β is the fluid volumetric expansion coefficient, F is the inertia coefficient, $k_{feff} = \varepsilon k_f$ and $k_{seff} = (1-\varepsilon)k_s$ are the effective fluid and solid thermal conductivities, respectively, h_{sf} is the interstitial heat transfer coefficient, ν_f is the fluid kinematic viscosity, ρ_f is the fluid density, T stands for temperature, $|\langle \mathbf{v}\rangle| = \sqrt{u^2+v^2}$ and $\mathbf{v}$ represents the interstitial velocity vector. Hereafter, the volume-average symbol $\langle\ \rangle$ will be dropped for convenience. The permeability of the porous medium is appraised by the dimensionless Darcy number. It has been argued that the convective term can be omitted in forced convection flows in porous media. However, its influence is retained in the current study to examine its impact on the momentum and energy transport processes inside the cavity.

With the two energy equations at hand, the effective thermal conductivity is defined separately for each phase. In carrying out this investigation, no slip velocity condition is imposed at the solid walls. Also, both fluid and solid phases are assumed in local thermal equilibrium at the solid walls. The mathematical model is completed by outlining the boundary conditions, which are $\mathbf{v} = 0$ at the walls, $T = T_h$ at $y = 0$, $T = T_c$ at $y = H$, $\partial T/\partial x = 0$ at $x = 0, L$. The selection of material properties was merely based on a wide spectrum of possible encountered engineering applications. It is convenient to cast the governing equations in terms of dimensionless variables such that

$$X = \frac{x}{H},\quad Y = \frac{y}{H},\quad Da = \frac{K}{H^2},\quad \mathbf{V} = \frac{\mathbf{v}H}{\alpha_m},$$
$$P = \frac{pH^2}{\rho\alpha_m^2},\quad Pr = \frac{\nu_f}{\alpha_f},\quad \theta = \frac{T-T_c}{T_h-T_c} \tag{5}$$

where Da is the Darcy number. The modified thermal diffusivity α_m is set equal to $k_m/(\rho c)_f$, where $k_m = \varepsilon k_f + (1-\varepsilon)k_s$. Upon employing the dimensionless variables, the governing equations can be written as

$$\nabla \cdot \mathbf{V} = 0 \tag{6}$$

$$\left(\frac{1+\kappa^{-1}}{\varepsilon Pr}\right)(\mathbf{V}\cdot\nabla\mathbf{V}) = -\nabla P + \frac{1}{\varepsilon}\nabla^2\mathbf{V} - \frac{1}{Da}\mathbf{V} - \frac{\varepsilon F(1+\kappa^{-1})}{PrDa^{1/2}}|\mathbf{V}|\mathbf{V} + \frac{Ra}{Da}\theta_f\mathbf{k} \tag{7}$$

$$(1+\kappa^{-1})(\mathbf{V}\cdot\nabla\theta_f) = \nabla^2\theta_f + \chi(1+\kappa^{-1})(\theta_s - \theta_f) \tag{8}$$

$$0 = \nabla^2\theta_s - \chi(1+\kappa)(\theta_s - \theta_f) \tag{9}$$

where χ, κ and Ra are, respectively, the modified Biot number, effective fluid-to-solid thermal conductivity ratio and Rayleigh–Darcy number given by

$$\chi = \frac{h_{sf}a_{sf}H^2}{k_m}, \quad \kappa = \frac{k_{feff}}{k_{seff}}, \quad Ra = \frac{g\beta(T_h - T_c)H^3}{\nu_f\alpha_m}Da \tag{10}$$

It should be pointed out that the modified Biot number χ (herein after referred to as Biot number) is defined as a function of k_m and not k_{feff} such that the implications of varying χ is isolated from the effect of κ to arrive at two independent dimensionless groups. In essence, the Biot number definition is a measure of the conduction thermal resistance offered by the porous medium over the interstitial convective thermal resistance between the two phases. What is more, the definition of the Rayleigh–Darcy (or Rayleigh number, for short) is consistent with the definition reported in the literature which emerges from natural convection Darcian flows in porous media. The total body force responsible for flow circulation is represented by Ra/Da. It should be pointed out that this body force term is related to the Rayleigh number for classical clear flows in the following manner:

$$\frac{Ra}{Da} = \frac{Ra_{\text{clear flow}}}{\varepsilon(1+\kappa^{-1})} \tag{11}$$

One may deduce from Eq. (7) that the body force term can be increased by either increasing the Rayleigh number, which provides a measure for the imposed temperature gradient ΔT, or decreasing the Darcy number, which is a measure of the permeability of the porous medium. Hence, a large value of Rayleigh number reflects an increase in buoyancy force strength, whereas a decrease in Darcy number signals a decrease in flow conductance. Eq. (7) will be referred herein after by the generalized form of the momentum equation.

In accordance with the problem description, it is instructive to outline the dimensionless boundary conditions which are given by

$$\begin{aligned}
&\mathbf{V} = (0,0) \quad \text{at } X = 0, A, \ 0 \leqslant Y \leqslant 1\\
&\mathbf{V} = (0,0) \quad \text{at } Y = 0, 1, \ 0 \leqslant X \leqslant A\\
&\theta_f = \theta_s = 1 \quad \text{at } Y = 0, \ 0 \leqslant X \leqslant A\\
&\theta_f = \theta_s = 0 \quad \text{at } Y = 1, \ 0 \leqslant X \leqslant A\\
&\frac{\partial\theta_f}{\partial X} = \frac{\partial\theta_s}{\partial X} = 0 \quad \text{at } X = 0, A, \ 0 < Y < 1
\end{aligned} \tag{12}$$

The steady state value of the local Nusselt number can be calculated by integrating the energy flow across a horizontal cross-section upon incorporating the dimensionless variables to arrive at the following expression

$$Nu = \frac{q_w H}{k_m(T_h - T_c)} = -\left[\frac{1}{(1+\kappa^{-1})}\frac{\partial\theta_f}{\partial Y} + \frac{1}{(1+\kappa)}\frac{\partial\theta_s}{\partial Y}\right]_{Y=0} \tag{13}$$

Similarly, the average Nusselt number can be written as

$$\overline{Nu} = \frac{-1}{A}\int_0^A \left[\frac{1}{(1+\kappa^{-1})}\frac{\partial\theta_f}{\partial Y} + \frac{1}{(1+\kappa)}\frac{\partial\theta_s}{\partial Y}\right]_{Y=0} dX \tag{14}$$

It is essential to use the effective thermal conductivities of the fluid and solid phase in the expression of the overage Nusselt number in order to obtain a more accurate and meaningful representation of the dimensionless heat transfer coefficient at the hot wall.

3. Numerical method and solution

The numerical solution of the transformed dimensionless momentum equations (6) and (7) and the two energy equations (8) and (9) are discretized using the finite volume (FV) method. All the dependent variables are solved for in cell-centered, co-located computational nodes. The surface and volume integrals of the conservation terms are evaluated using the mid-point approximation. In order to handle the encountered stiffness of the non-linear system, the convective flux is discretized using the second-order central differencing scheme (CDS) that is coupled with an upwind differencing scheme (UDS) via the 'deferred correction' technique. In this technique, the low-order, but stable, flux attained using UDS contributes to the matrix coefficients and the difference between the fluxes obtained using CDS and UDS contributes to the source term so that CDS-flux will eventually prevail upon the convergence. Furthermore, the CDS is used to discretize the diffusive flux. In order to preserve a compact and structured computational molecule of the linearized equations, all flux contributions that would result in off-diagonal matrix coefficients are taken care of as deferred source terms. The SIMPLEX algorithm for the pressure–velocity coupling is used. In applying this algorithm, the cell face velocities needed to impose the mass conservation constraint, that drives the pressure and velocity correction, are obtained via a linear momentum interpolation as described by Rhie and Chow [23].

The source term in the motion equation is linearized in such a way that will ensure diagonal dominance in the corresponding discretized equation (see [19]). Moreover, the Darcian and the quadratic velocity source terms in the U-momentum equation, for example, can be expressed as

$$S_V = S_c - S_p V - \frac{Ra}{Da}\theta_f = -\frac{1}{Da}V - \frac{\varepsilon F(1+\kappa^{-1})}{PrDa^{1/2}}(U^2+V^2)^{1/2}V - \frac{Ra}{Da}\theta_f \tag{15}$$

As a result, the coefficients S_c and S_p are given as

$$S_c = \frac{\varepsilon F(1+\kappa^{-1})}{PrDa^{1/2}}(U^2+V^2)^{-1/2}V^3 - \frac{Ra}{Da}\theta_f \quad (16)$$

$$S_p = \frac{1}{Da} + \frac{\varepsilon F(1+\kappa^{-1})}{PrDa^{1/2}}[(U^2+V^2)^{-1/2}U^2 + (U^2+V^2)^{1/2}] \quad (17)$$

Such a representation as outlined above ensures that S_p is always positive and therefore satisfies the boundedness condition, which is considered sufficient for convergence. The resulting systems of the algebraic motion and energy equations are solved using the simply implicit procedure (SIP) as outlined by Ferziger and Peric [24]. Since velocity and temperature fields are coupled in the undergoing investigation, the motion followed by the energy equations are solved iteratively until both the change in velocities and temperature solutions as well as mass imbalance fall below 10^{-6} at all nodes.

In order to improve the convergence rate, a coarse correction technique is used. In this technique, three grid levels, which are refined sequentially by slicing it in half in both spatial dimensions, are employed. The solution obtained using a coarser grid is interpolated (prolonged) to initialize the solution on the finer grid. Furthermore, the third grid level constitutes of 250×50 quadrilateral control volumes distributed along X and Y coordinates, respectively. Grid clustering near the walls is obtained using 0.05% stretching from the mid-lines crossing the cavity. It is worth mentioning that the fourth grid level refinement (500×100) lead to insignificant changes in the obtained solution. Finally, the local and average Nusselt number predictions a long the top and bottom walls is depicted in Fig. 2 using the Darcy model for $Ra = 50$, $\kappa = 0.1$, $\chi = 10$ and $Da = 10^{-3}$. As can be seen form the figure, the results show excellent agreement at both stated heights to within 10^{-6} relative difference, which boosts the confidence in our numerical code.

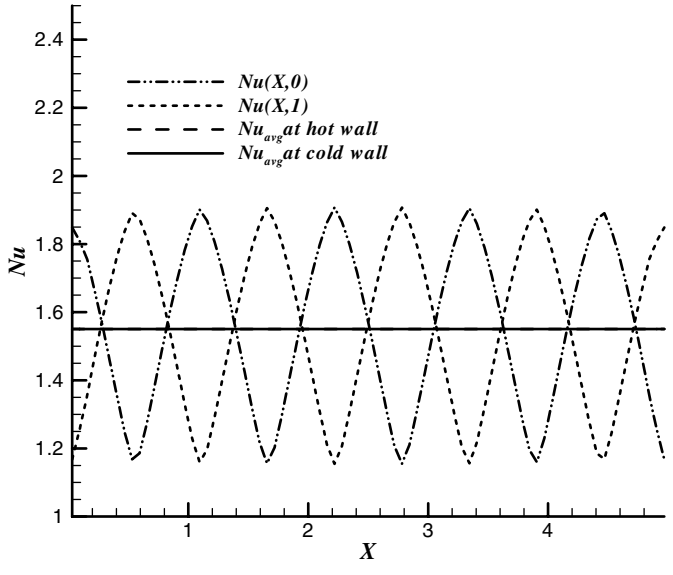

Fig. 2. Assessment of the local and average Nusselt number predictions using the Darcy model for $Ra = 50$, $\kappa = 0.1$, $\chi = 10$ and $Da = 10^{-3}$.

4. Results and discussion

The prime objective of the current work, as stated earlier, is to gauge the magnitude of the local thermal non-equilibrium (LTNE) model over a broad range of dimensionless groups that represent possible operating conditions encountered in engineering applications. These dimensionless groups and their operating envelopes are the Rayleigh number $1 \leqslant Ra \leqslant 400$, Darcy number $10^{-4} \leqslant Da \leqslant 10^{-3}$, dimensionless effective fluid-to-solid thermal conductivity ratio $0.1 \leqslant \kappa \leqslant 1.0$, and modified Biot number $1 \leqslant \chi \leqslant 100$. In the current numerical work, the flow circulation intensity is also documented, which is associated with the magnitude of LTNE model. In this regard, the flow intensity could be better represented by introducing the dimensionless stream function Ψ given by

$$U = \frac{\partial \Psi}{\partial Y}, \quad V = -\frac{\partial \Psi}{\partial X} \quad (18)$$

which allows for a single representation of flow behavior instead of the velocity components. It is worth noting that the negative and positive Ψ values indicate clockwise and counter-clockwise cells, respectively.

The LTNE model can be quantified to serve as an assessment tool for examining the validity range of local thermal equilibrium. This is achieved here by determining the absolute value of the local temperature difference between the fluid and solid phase in the entire cavity such that

$$\mathrm{LTNE} = |\theta_s - \theta_f| \quad (19)$$

The sensitivity of the LTNE model was documented by recording the maximum values of both the flow intensity and LTNE for each particular case study. It should be pointed out that the significance of LTNE value would ultimately depend on the application at hand, where porous media applications involving higher risk margins do not tolerate a large LTNE value.

The current work preludes by weighing the sensitivity of the various non-Darcian terms listed in the momentum equation, i.e., Eq. (7), against the generalized form of the momentum equation. When relaxing one or more of the non-Darcian terms, the following momentum transport models arise: Darcy (D) model, Darcy–Brinkman (DB) model, and Darcy–Brinkman with flow convection (DBC) model, i.e., the generalized model without the Forchhiemer term. Hence, the generalized momentum equation will encompass all the considered non-Darcian effects in this investigation and will be referred to as DBFC model. It is imperative to understand the significance and contribution of each of the non-Darcian term in a laminar natural convection heat transfer in a cavity setting. Hence, the different presented models will shed light on such

non-Darcian effects under a wide range of *Ra* values. In natural convection heat transfer applications with the configuration at hand, a prescribed *Ra* value sets the magnitude of the flow activities induced by the buoyancy forces, which are in turn sustained by the imposed temperature gradient.

It is a mere fact that the Darcy model predicts the highest velocity value at any given *Ra* value owing to negligence of flow impedance terms such as the solid boundary effect and the Forchhiemer inertial effect. Furthermore, the Brinkman term, which accounts for the solid boundary, forces the no-slip condition at the walls. Such an effect would reduce the predicted velocity when employing the DB model. Also, inclusion of the convective term aids flow motion and, hence, increases the velocity magnitude predicted upon employing the Darcy–Brinkman model with the convective term, i.e., DBC model. Finally, the Forchhiemer term, which accounts for resistance to flow offered by the presence of the solid structure, retards flow motion and suppresses flow circulation especially at elevated flow speeds. On the contrary, silencing the Forchhiemer term assists in enlarging the discrepancies between the different tackled case studies. Owing to the massive results generated in the current numerical investigation, representative results will be presented for brevity. The DBC model will be taken as the default for the presented case studies unless otherwise stated.

Fig. 3 illustrates the streamlines, fluid and solid isotherms and LTNE contours for $\kappa = 0.1$, $\chi = 10$ and $Da = 10^{-3}$ using the DBC model. Results are shown for $Ra = 50$ and $Ra = 400$. The Bénard convection is clearly displayed by the repeated rotating cells with '+' and '−' symbols on the streamlines representing clockwise and counter-clockwise rotation direction, respectively. As the Rayleigh number increases from 50 to 400, the flow activities intensify owing to the increase in the sustained buoyancy forces. This observation is manifested in the elevation of the streamlines strength when increasing *Ra* values. It is also observed that the number of cells has been reduced eight to six as the operating domain per cell is seen to be stretched from a length of about half a cavity height to a full cavity height. Fig. 3 also displays the distribution

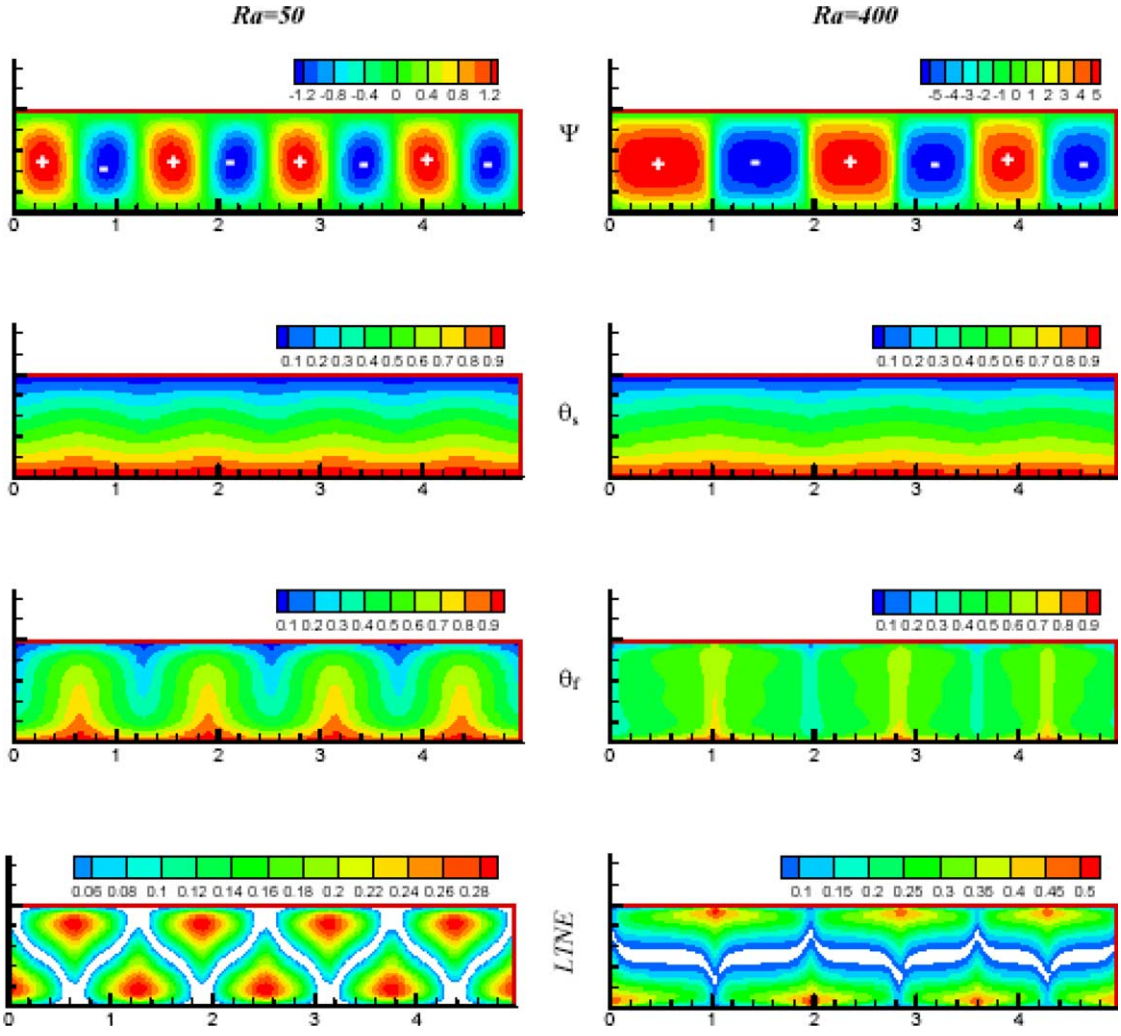

Fig. 3. Contours of the streamline, solid temperature, fluid temperature and LTNE using the DBC model with $\kappa = 0.1$, $\chi = 10$, $Da = 10^{-3}$ and Rayleigh numbers of 50 and 400, respectively.

of fluid and solid temperatures over the entire cavity for $Ra = 50$ and $Ra = 400$. The solid temperature contours seems to be stabilized even at $Ra = 400$, which is likely accredited to the relatively larger energy transport coefficient, i.e., k_{seff} attained by the solid. On the contrary, thermal plumes are observed in the fluid temperature distribution. Such plumes occur at lengths corresponding to the interface of two consecutive opposite rotating cells. However, the thermal plumes are noticed to diminish with the increase in Ra value owing to the increase in flow intensity. The LTNE layout also reflects the repeated cells formation across the length of the cavity. The white domains represent LTNE values below 0.05, which can be viewed as the upper constraint of LTE validity. As can be seen form the figure, the highest recorded exists at positions corresponding to the tip of the thermal plumes offered by the fluid temperature distribution. Meanwhile, it is vivid that higher encountered flow activities bring about more isotherm discrepancies between the two phases as demonstrated by the larger magnitudes of LTNE values arrived at $Ra = 400$. It is worth noting that the validity of LTE condition, based on the above declared criterion, can be justified at $Ra = 400$ in the core of the cavity and between the opposite rotating cells underneath the thermal plumes pictured in the fluid isotherms.

Fig. 4 displays the maximum recorded Ψ strength for each of the four models at hand. The results illustrate the positive values of Ψ as the magnitude of the negative and maximum of Ψ is almost the same for the configuration considered in the current investigation. The results show that the computed stream function values by all the models fall in close proximity up to a Rayleigh number of 20, which corresponds to a prevailing conduction heat transfer regime. Beyond this critical value, the results show that the largest $\Psi_{\max}$ values are obtained using the Darcy (D) model while the lowest is furnished by the generalized (DBFC) model. Furthermore, the convective term does not seem to have a significant impact on the recorded $\Psi_{\max}$ strength while the DBFC model tends to shy below due to the flow impedance offered primarily by the Forchhiemer term. Such depreciation in the velocity prediction by the DBFC model becomes more pronounced at elevated Ra values owing to the quadratic nature of the Forchhiemer term. Although some might be tempted in resorting to the Darcy model owing to its simplicity, caution should be exercised giving that the model over predicts the actual flow motion inside a porous medium, especially at elevated Ra values. For instance, the discrepancy in the predicted $\Psi_{\max}$ values between the Darcy model and the DBFC

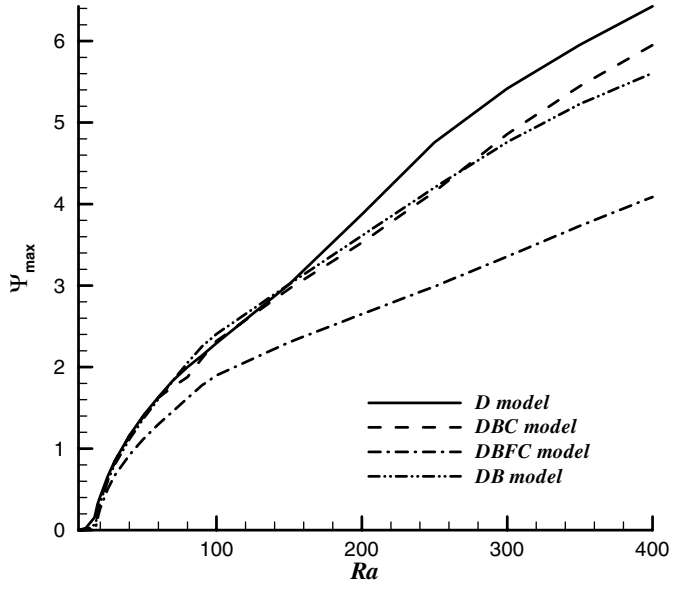

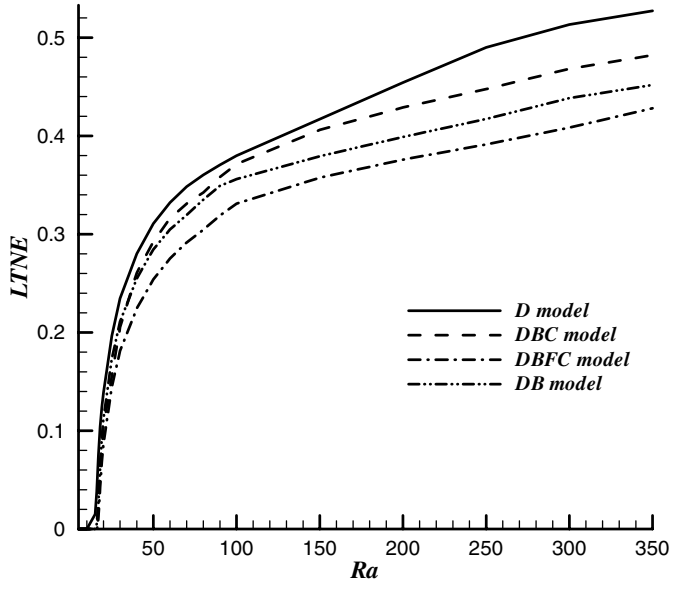

Fig. 4. Impact of Rayleigh number on flow intensity and LTNE using the DBC model with $\kappa = 0.1$, $\chi = 10$ and $Da = 10^{-3}$.

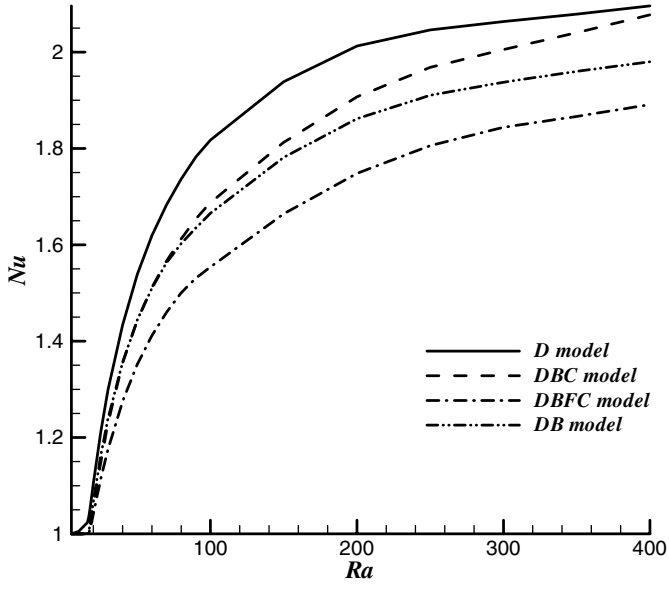

Fig. 5. Average Nusselt number predictions at different Rayleigh numbers using the DBC model with $\kappa = 0.1$, $\chi = 10$ and $Da = 10^{-3}$.

model magnifies from 22% to 60% upon increasing *Ra* value from 100 to 400, respectively. In addition, Fig. 4 presents the magnitude of the maximum LTNE values, as defined in Eq. (19), in the considered *Ra* domain. It is obvious that the Forchhiemer term is the most crucial factor in suppressing LTNE value at elevated *Ra* values. In fact, the elimination of the Forchhiemer term expands the sustained temperature difference between the two phases due to augmentation of interstitial convective heat transfer communication between them. Moreover, it can be seen that the largest recorded LTNE value at a prescribed *Ra* value corresponds to the model with the highest predicted flow motion, i.e., the Darcy model. Accordingly, one may deduce that a higher flow motion agitates LTNE value. Moreover, it is worth noting that the critical *Ra* value, which signals the onset of natural convection, was found to be less than 20 for all the considered models.

Fig. 5 demonstrates the computed average Nusselt number at different *Ra* values. Apparently, the Darcy model assumes the relatively largest magnitude of convection current in the cavity. Consequently, the highest average Nusselt number is furnished by the Darcy model and the lowest by DBFC model. Such an observation is more pronounced at high *Ra* values. The convective term appears to slightly improve Nusselt number predictions while the Forchhiemer term tends to significantly retard flow motion.

Fig. 6 demonstrates the effect of Darcy number on the flow circulation and LTNE condition using $\kappa = 1.0$, $\chi = 100$. Again, the Darcy number serves as an indicator that reflects the permeability of the porous medium. Here, the effect of Darcy number is more meaningfully sensed by plotting the considered sought dependent variables against Ra/Da, where the effect of Darcy number is stripped from *Ra* definition. The results clearly show that a higher flow intensity is associated with a larger considered *Da* value (i.e., $Da = 10^{-3}$). The enhanced flow conductance permits higher circulation through the porous openings, which subsequently triggers the onset of natural convection at a lower *Ra* value. This is turn augments the interstitial convective heat transfer communication between the two phases, which results in elevating the LTNE magnitude with the increase in *Da* value. Moreover, Fig. 7 illustrates the improvement in the average Nusselt number predictions over the *Ra* range owing to the increase in *Da* value. Such an observation is consistent with published reports in the literature.

Fig. 8 captures the impact of the effective fluid-to-solid thermal conductivity ratio κ on LTNE condition using $\chi = 100$ and $Da = 10^{-3}$. Higher flow circulation is recorded for $\kappa = 1.0$ as the fluid transport coefficient contributes to

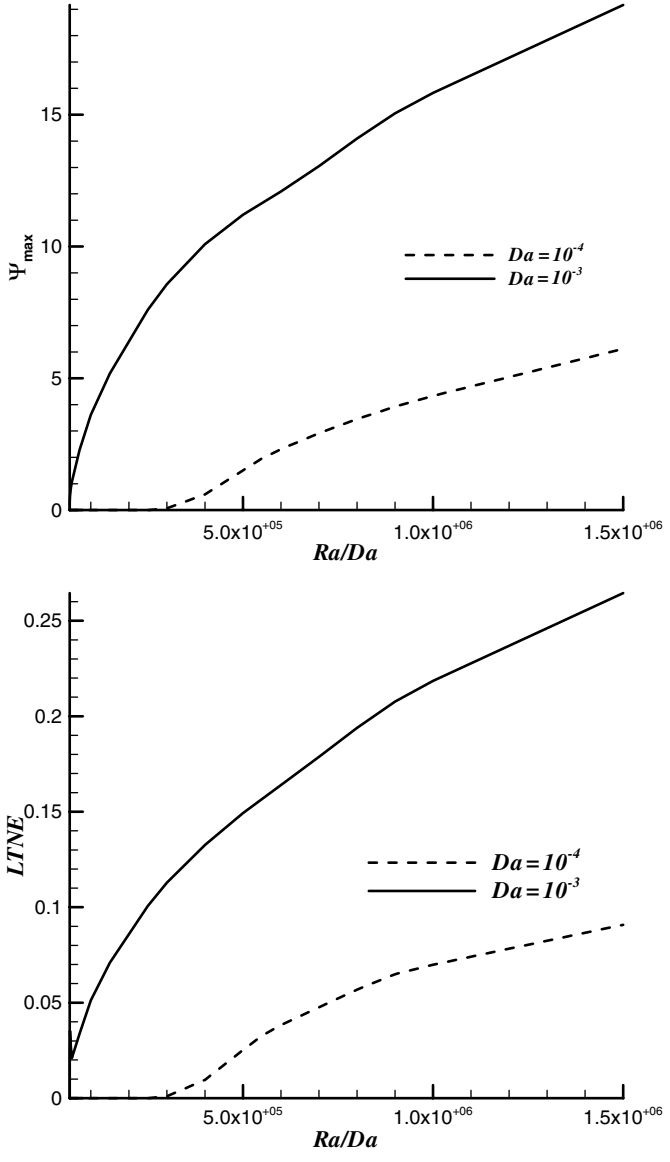

Fig. 6. Impact of Darcy number on flow intensity and LTNE condition using the DBC model with $\kappa = 0.1$, $\chi = 10$ and $Da = 10^{-3}$.

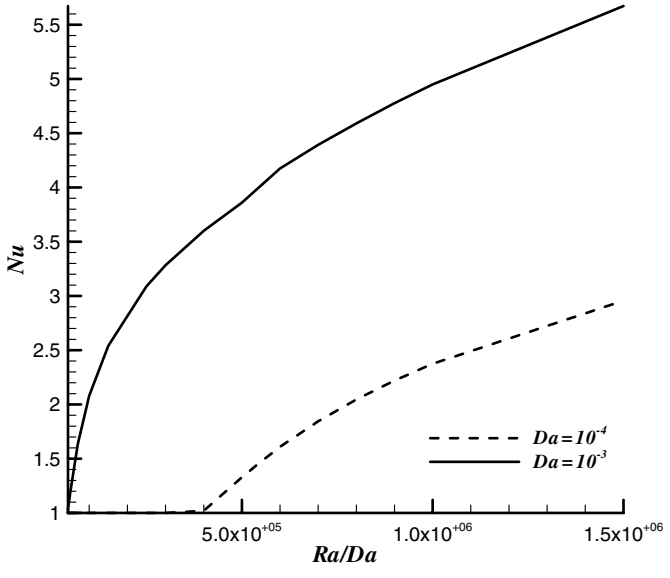

Fig. 7. Effect of Darcy number on the average Nusselt number predictions using the DBC model with $\kappa = 0.1$, $\chi = 10$ and $Da = 10^{-3}$.

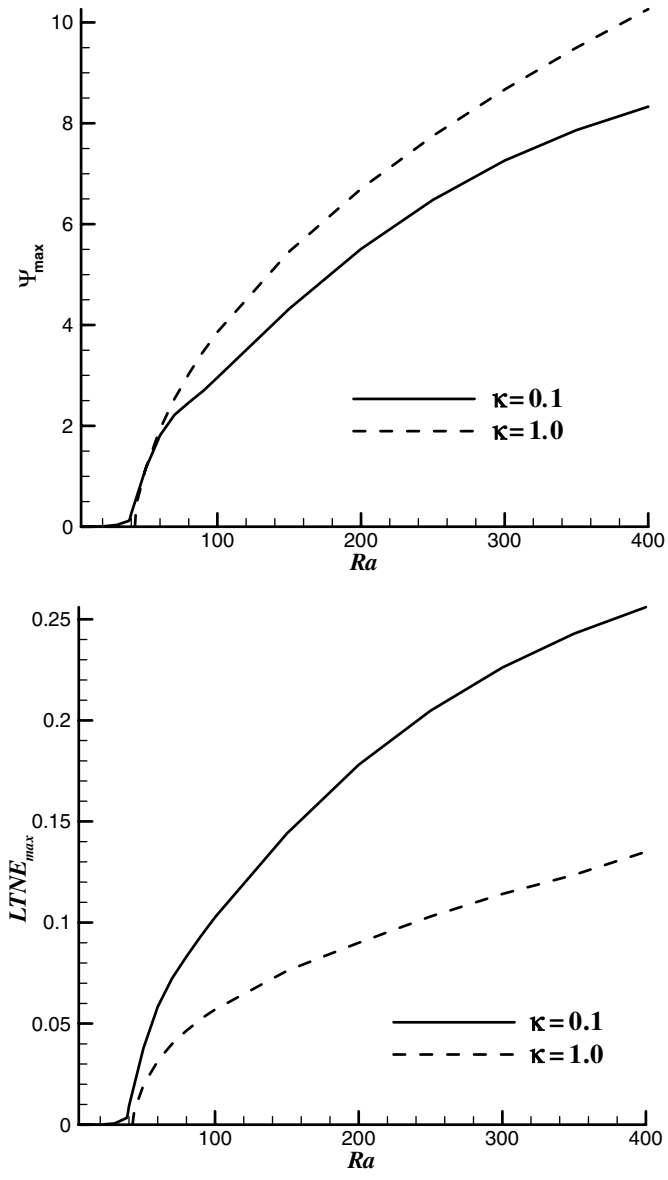

Fig. 8. Impact of κ value on flow intensity and LTNE condition at different Rayleigh numbers using the DBC model with $\chi = 100$ and $Da = 10^{-3}$.

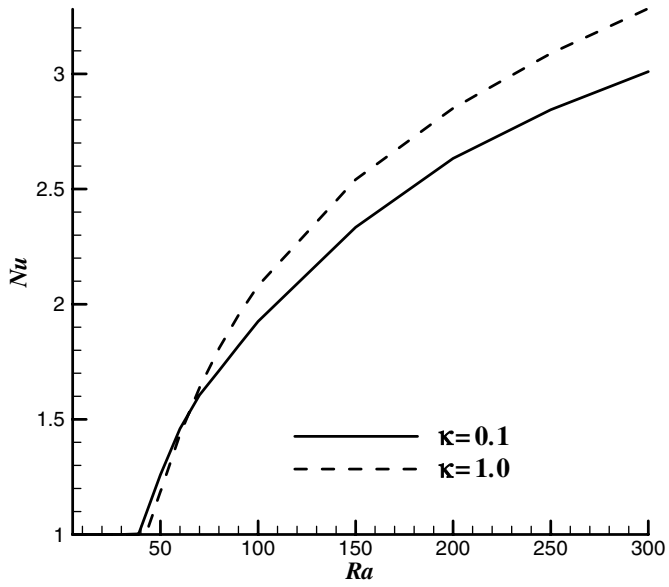

Fig. 9. Effect of κ value on the average Nusselt number predictions at different Rayleigh numbers using the DBC model with $\chi = 100$ and $Da = 10^{-3}$.

the buoyancy driven activities and, hence, to the flow circulation. Furthermore, increasing the κ value indicates that the fluid is becoming more capable of exchanging energy, i.e., better energy carrier from the hot wall to the porous medium. Accordingly, it confines the local temperature discrepancy between the two phases, which announces the suppression of LTNE value with the increase in κ value. It is worth noting that the difference attained in the LTNE value generated between $\kappa = 0.1$ and $\kappa = 1.0$ remains almost the same over the considered over the *Ra* range after exceeding the critical *Ra* value. Moreover, Fig. 9 displays higher average Nusselt number predictions when incorporating $\kappa = 1.0$ instead of $\kappa = 0.1$. This is likely attributed to the increase in flow circulation as shown in the previous figure.

The current investigation is concluded by highlighting the effect of the Biot number χ using $\kappa = 0.1$ and $Da = 10^{-3}$. The results are first depicted for the effect of the Biot number on the flow intensity and LTNE as demonstrated in Fig. 10. The onset of natural convection is found to be initiated first when incorporating the lowest considered χ value, i.e., $\chi = 1$. However, it is manifested that the rate at which circulation increases with increasing *Ra* is higher when considering the largest χ value, i.e., $\chi = 100$. Fig. 10 also depicts the maximum LTNE value plotted against *Ra* for different χ values. The results show that LTE condition is approached with an increase in χ value. This is attributed to the enhanced communication between the two phases at the expense of the modified effective thermal conductivity of the porous medium k_m. Finally, the average Nusselt number at various *Ra* values is displayed in Fig. 11 using $\kappa = 0.1$ and $Da = 10^{-3}$. It is clear that the onset of natural convection is delayed with the increase in χ value. While the natural convection contribution to overall heat transfer takes effect almost immediately at $\chi = 1$ such a contribution is delayed to roughly $Ra = 39$ when employing $\chi = 100$. It is noticed, however, that the enhancement in the average Nusselt number upon employing larger χ values climbs a steeper slope with the increase in Rayleigh number.

5. Conclusions

The present numerical simulation is concerned with modeling the steady state behavior of a natural convection heat transfer inside an enclosed cavity. The cavity is essentially two-dimensional and is filled with a fluid-saturated porous medium. In addition, the fluid is considered to be incompressible that operates in the laminar regime,

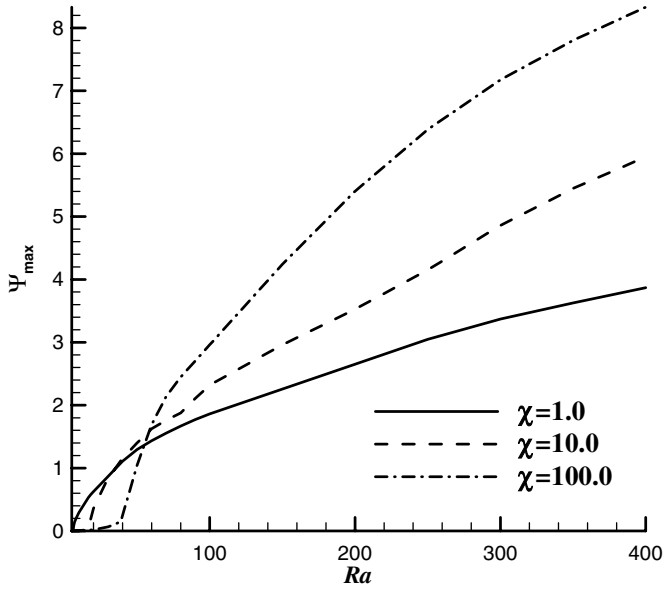

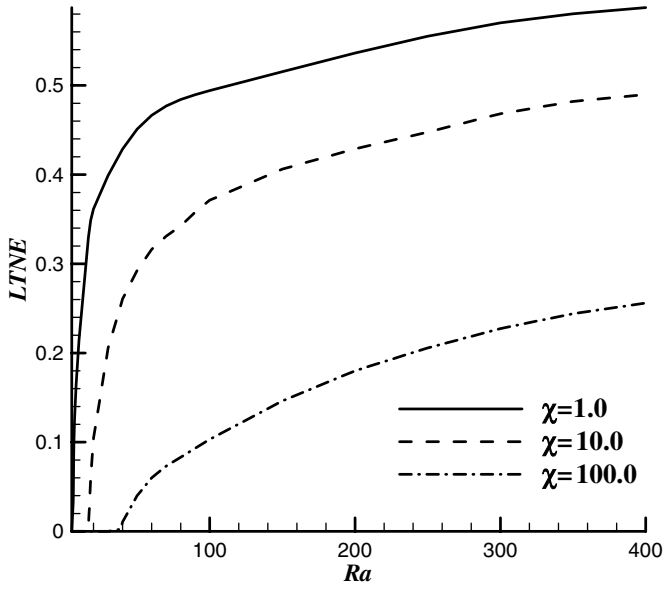

Fig. 10. Impact of Biot number χ on flow intensity and LTNE condition at different Rayleigh numbers using the DBC model $\kappa = 0.1$ and $Da = 10^{-3}$.

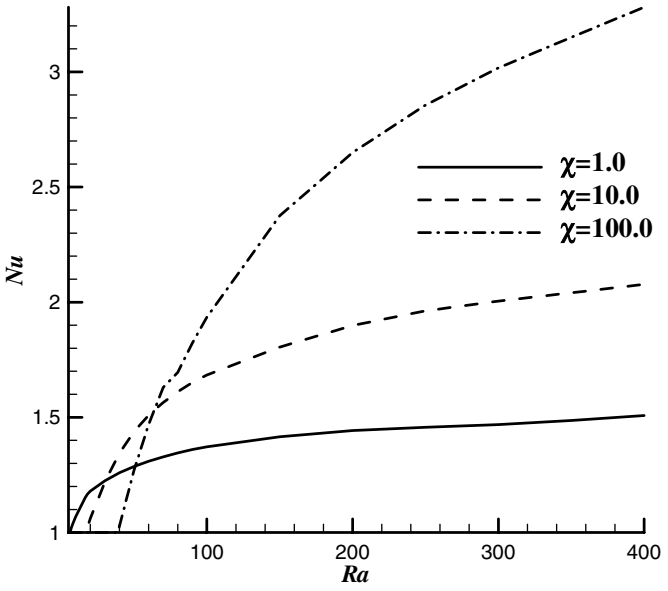

Fig. 11. Effect of Biot number χ on the average Nusselt number predictions at different Rayleigh numbers using the DBC model with $\kappa = 0.1$ and $Da = 10^{-3}$.

whereas the porous medium is considered to be homogenous and isotropic. The thermophysical properties were assumed to be constant except for the density term rising in the buoyancy term which is handled according to Boussinesq formulation. Furthermore, the bottom wall was subjected to a relatively higher temperature than the top wall, whereas the vertical walls were considered to be insulated. The generalized form of the momentum equation is employed while provisions are made to examine the individual non-Darcian parameters, which constitute the momentum equation. Moreover, the representation of the local fluid and solid temperatures were accounted for separately by employing the two-energy equation model. Also, the heat transfer between the fluid and solid phase was assumed to be solely comprised of a convective mode. Several dimensionless groups were employed in a selected operating envelope that corresponds to actual engineering applications. These dimensionless groups are the Rayleigh number $1 \leqslant Ra \leqslant 400$, Darcy number $10^{-4} \leqslant Da \leqslant 10^{-3}$, effective fluid-to-solid thermal conductivity ratio $0.1 \leqslant \kappa \leqslant 1.0$, and the modified Biot number $1 \leqslant \chi \leqslant 100$.

The chief objective of the current numerical investigation was to obtain a better understanding of the local temperature discrepancy between the two phases through introducing the LTNE condition. This condition was studied in conjunction with the impact of the various dimensional groups on flow circulation intensity and average Nusselt number predictions. Such an understanding paves the path for identifying domains where the local thermal equilibrium (LTE) assumption can be considered valid within a reasonable accuracy based on the application at hand.

Amongst the different tackled flow transport models, the effect of Forchhiemer term was found to be more pronounced at high *Ra* values. Moreover, the generalized model was found to predict the lowest velocity magnitude (due to incorporation of various non-Darcian effects), whereas the Darcy model was predicting the highest velocity magnitude at any given *Ra* value. The results also show that an elevation in Rayleigh number enhances flow circulation and LTNE value, which ultimately results in an increase in the average Nusselt number predictions. In addition, the decrease in Darcy number impedes flow circulation and brings about depreciation in the average Nusselt number predictions. It also diminishes interstitial heat transfer communication between the two phases. Thus, lower LTNE values were observed with a decrease in *Da* value. Next, the LTNE value was found to depreciate with

an increase in the effective fluid-to-solid thermal conductivity ratio κ. Finally, the increase of the Biot number χ was found to improve the local thermal equilibrium assumption and the average Nusselt number predictions.

Acknowledgement

The first author acknowledges the financial support received from the Research Affairs at the UAE University under contract number 06-05-7-11/04.

References

[1] D.A. Nield, A. Bejan, Convection in Porous Media, second ed., Springer, Berlin, 1999.
[2] D.B. Ingham, I. Pop (Eds.), Transport Phenomena in Porous Media, vol. 2 (2002), Pergamon, Oxford, 1998.
[3] K. Vafai (Ed.), Handbook of Porous Media, Marcel Dekker, New York, 2000.
[4] I. Pop, D.B. Ingham, Convective Heat Transfer: Mathematical and Computational Modelling of Viscous Fluids and Porous Media, Pergamon, Oxford, 2001.
[5] A. Bejan, A.D. Kraus (Eds.), Heat Transfer Handbook, Wiley, New York, 2003.
[6] D.B. Ingham, A. Bejan, E. Mamut, I. Pop (Eds.), Emerging Technologies and Techniques in Porous Media, Kluwer, Dordrecht, 2004.
[7] A. Bejan, I. Dincer, S. Lorente, A.F. Miguel, A.H. Reis, Porous and Complex Flow Structures in Modern Technologies, Springer, New York, 2004.
[8] E.R. Lapwood, Convection of a fluid in a porous medium, Proc. Camb. Philos. Soc. 44 (1948) 508–521.
[9] M. Kaviany, Principles of Heat Transfer in Porous Media, Springer-Verlag, New York, 1991.
[10] B.K.C. Chan, C.M. Ivey, J.M. Barry, Natural convection in enclosed porous media with rectangular boundaries, J. Heat Transfer 92 (1970) 21–27.
[11] G. Lauriat, V. Prasad, Bénard convection in porous media: non-Darcian effects on natural convection in a vertical porous enclosure, Int. J. Heat Mass Transfer 32 (1989) 2135–2148.
[12] J.G. Georgiadis, I. Catton, Prandtl number effect on Bénard convection in porous media, J. Heat Transfer 108 (1986) 284–290.
[13] J.L. Lage, A. Bejan, J.G. Georgiadis, The Prandtl number effect near the onset of Bénard convection in a porous medium, Int. J. Heat Fluid Flow 13 (1992) 408–411.
[14] P. Vasseur, C.H. Wang, M. Sen, The Brinkman model for natural convection in a shallow porous cavity with uniform heat flux, Numer. Heat Transfer: Part (A) 15 (1989) 221–242.
[15] H. Beji, D. Gobin, Influence of thermal dispersion on natural convection heat transfer in porous media, Numer. Heat Mass Transfer: Part (A) 22 (1922) 487–500.
[16] A.M. Al-Amiri, Natural convection in porous enclosures: the application of the two-energy equation model, Numer. Heat Transfer: Part (A) 41 (2002) 817–834.
[17] K. Vafai, C.L. Tien, Boundary and inertia effects on flow and heat transfer in porous media, Int. J. Heat Mass Transfer 108 (1981) 195–203.
[18] S. Khashan, A. Al-Amiri, M. Al-Nimr, Assessment of the local thermal non-equilibrium condition in developing forced convection flows through fluid-saturated porous tubes, Appl. Therm. Eng. 25 (2005) 1429–1445.
[19] A.M. Al-Amiri, Analysis of momentum and energy transfer in a lid-driven cavity filled with a porous medium, Int. J. Heat Mass Transfer 43 (2000) 3513–3527.
[20] A. Amiri, K. Vafai, Analysis of dispersion effects and non-thermal equilibrium, non-Darcian, variable porosity incompressible flow through porous media, Int. J. Heat Mass Transfer 11 (1994) 939–954.
[21] A. Amiri, K. Vafai, Transient analysis of incompressible flow through a packed bed, Int. J. Heat Mass Transfer 41 (1998) 4259–4279.
[22] K. Vafai, A. Amiri, Thermal non-equilibrium forced convection in porous media, in: D.B. Ingham, I. Pop (Eds.), Transport Phenomena in Porous Media, vol. 1, Pergamon, Amsterdam, 1998, pp. 313–329.
[23] C. Rhie, W. Chow, Numerical study of the turbulent flow past an airfoil with trailing edge separation, AIAA J. 21 (1983) 1525–1532.
[24] J.H. Ferziger, M. Peric, Computational Methods for Fluid Dynamics, Springer-Verlag, New York, 1999.